



# Tunable viscosity modification with diluted particles: when particles decrease the viscosity of complex fluids

Manuchar Gvaramia<sup>1,2</sup> · Gaetano Mangiapia<sup>3</sup> · Vitaliy Pipich<sup>1</sup> · Marie-Sousai Appavou<sup>1</sup> · Sebastian Jaksch<sup>1</sup> · Olaf Holderer<sup>1</sup> · Marina D. Rukhadze<sup>4</sup> · Henrich Frielinghaus<sup>1</sup>

Received: 17 July 2019 / Revised: 5 September 2019 / Accepted: 7 September 2019 / Published online: 27 October 2019  
© The Author(s) 2019

## Abstract

While spherical particles are the most studied viscosity modifiers, they are well known only to increase viscosities, in particular at low concentrations of approx. 1%. Extended studies and theories on non-spherical particles in simple fluids find a more complicated behavior, but still a steady increase with increasing concentration. Involving platelets in combination with complex fluids—in our case, a bicontinuous microemulsion—displays an even more complex scenario that we analyze experimentally and theoretically as a function of platelet diameter using small angle neutron scattering, rheology, and the theory of the lubrication effect, to find the underlying concepts. The clay particles effectively form membranes in the medium that itself may have lamellar aligned domains and surfactant films in the case of the microemulsion. The two-stage structure of clay and surfactant membranes explains the findings using the theory of the lubrication effect. This confirms that layered domain structures serve for lowest viscosities. Starting from these findings and transferring the condition for low viscosities to other complex fluids, namely crude oils, even lowered viscosities with respect to the pure crude oil were observed. This strengthens our belief that also here layered domains are formed as well. This apparent contradiction of a viscosity reduction by solid particles could lead to a wider range of applications where low viscosities are desired. The same concepts of two-stage layered structures also explain the observed conditions for extremely enhanced viscosities at particle concentrations of 1% that may be interesting for the food industry.

**Keywords** Complex fluid · Clay · Rheology · Small angle neutron scattering

## Introduction

The demand of viscosity modifications by solid particles has many applications in the field of food science [1] and oil recovery [2]. An early theoretical model for diluted spherical particles

was developed by Einstein [3]. At that point, the predicted changes of the viscosity were small, especially for large dilutions in the concentration range of 1%wt. However, applications usually operate either at large concentrations (as in the case of chocolate [4]) or with asymmetric particles, such as clay platelets, which has many uses [5]. Therefore, more complicated theoretical concepts were developed [6, 7] dealing with competing hydrodynamic and colloidal interactions. The sometimes unknown balance of those leads to uncertain interpretations. Thus, the complicated case of particle concentrations much higher than 1% is out of the focus of this manuscript.

The medium in most published examples has been assumed to be a simple (Newtonian) liquid, such as water. However, the response of complex fluids [8, 9] to particles [10, 11] can be more complicated [12, 13]. In our past studies, we have studied the lubrication effect, which describes the lamellar ordering [14] of a complex fluid, i.e., a bicontinuous microemulsion ( $\mu$ E) next to a hydrophilic wall. This lamellar ordering allows the domains for facilitated sliding along the surface [13] (Fig. 1). In neutron scattering studies, we have

---

**Electronic supplementary material** The online version of this article (<https://doi.org/10.1007/s00396-019-04567-6>) contains supplementary material, which is available to authorized users.

---

✉ Henrich Frielinghaus  
h.frielinghaus@fz-juelich.de

<sup>1</sup> Jülich Centre for Neutron Science at MLZ, Forschungszentrum Jülich GmbH, Lichtenbergstrasse 1, 85747 Garching, Germany

<sup>2</sup> Department of Inorganic and Analytical Chemistry, University of Geneva, 30 Quai Ernest-Ansermet, 1205 Geneva, Switzerland

<sup>3</sup> Helmholtz Zentrum Geesthacht, Outstation at MLZ, 85747 Garching, Germany

<sup>4</sup> Department of Chemistry, Ivane Javakishvili Tbilisi State University, Chavchavadze Ave. 3, 380028 Tbilisi, Georgia

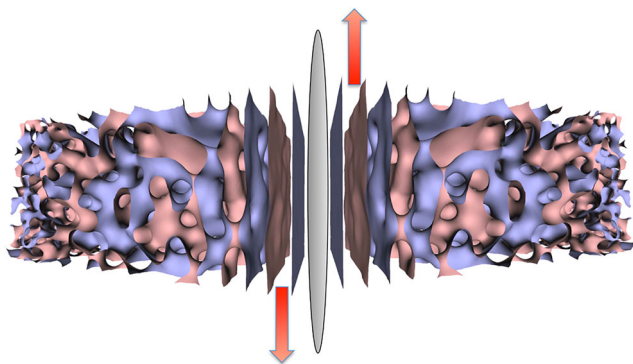


**Fig. 1** A sketch of the near platelet ordering of a complex fluid (i.e., of a bicontinuous microemulsion) in a shear field.

found that the typical relaxation times in these lamellae are faster than in the bulk. So, for platelet particles, a facilitated flow behavior (lower viscosity) might be expected [12]. The change of platelet diameters revealed that the perfection of lamellar modes increases with increasing platelet diameter [12]. Consequently, large platelets would serve the aim of reducing viscosity better than small ones. All particles are assumed to be wetted well due to the low surface tension [15]. On top, back coupling of the particles to the flow—such as alignment and/or tumbling—might be possible. All described effects must not be confused with the Lotus effect where the wetting is incomplete [16].

We recall theoretical concepts with different backgrounds and assumptions. Then we show structural studies using SANS and rheological measurements on well-defined clay systems with the simple fluid water and with a bicontinuous microemulsion. After that, two crude oils are presented that display a viscosity decrease at low temperatures. We rationalize the findings in the discussion and conclude.

## Experimental

**Materials** Clay particles were obtained from Süd Chemie (Rockwood), now belonging to the BYK chemicals group. We received four types of clay: Laponite RD that is reported to have a diameter of 25–30 nm, Laponite OG that is reported to have a diameter of 80 nm, Laponite WXFN that is reported to have a diameter of 140 nm, and Montmorillonite EXM 757 had a diameter of approx. 500 nm (all numbers from producers). The laponite materials were used without further cleaning. The montmorillonite material was dispersed in deionized water by sonication over-night and centrifuged, and the liquid portion was dried using a rotor vap and a vacuum oven. The particle characteristics are summarized in Table 1. The polydispersity for Laponite RD was reported to be in the  $\pm 5$  nm range, and for natural montmorillonite in the  $\pm 25\%$  range [17], which might be reduced by the cleaning

procedure. We assume a density of  $2.6 \text{ g/cm}^3$  for all clays when calculating the volume fractions [18].

N-decane and NaCl were obtained from Sigma Aldrich. The surfactant  $C_{10}E_4$  was obtained from Bachem, Weil am Rhein, Germany. Deuterated n-decane and heavy water were obtained from Armar chemicals, Döttingen, Switzerland. All these chemicals were used without further purification. Deionized water was obtained from the Purelab Ultra filter from ELGA at  $18.2 \text{ M}\Omega\text{cm}$ . The crude oils from Pennsylvania and Colorado (Denver basin) were obtained from ONTA Inc., Toronto, Canada. They were used as received.

One percent volume of clay dispersions was obtained by mixing the clay with deionized water and 1%wt NaCl, and sonication over-night. One percent weight of clay (total) and 1%wt NaCl (per water) were also dispersed in a microemulsion with a stock of 17%vol  $C_{10}E_4$ , 41.5%vol water, and 41.5%vol n-decane. The rendered salinity of the liquids exceeds the typical natural salinity from the clay by more or about three orders of magnitude (typically approx. 1 mEq of free charges are added by the dispersed clay [19] and thus can be neglected). The selected salinity screens the surface charges of the platelets to a large extent before coagulation of the platelets sets in [20, 21]; so the platelets are closest to pure steric repulsions. The symmetric microemulsion is bicontinuous and is located in the so-called fish tail (i.e., 1-phase region) when plotting temperature vs. surfactant content [22]. For neutron measurements, we used heavy water for the aqueous clay dispersion and the bulk contrast in the microemulsion samples. Film contrast with deuterated n-decane and heavy water was investigated as well—but no useful results emerged, and are omitted in this manuscript.

From simulations [23, 24] and experiments (citations therein), the contact angle of water/oil or water/ $\text{CO}_2$  against silica surfaces is in the range of  $0^\circ$  (fully wetted by water) over  $20$  to  $30^\circ$  (higher angles obtained by  $\text{CH}_3$ -functionalization). Thus, the preferential wetting of water on the clay particles can be safely assumed. The symmetric case of hydrophobic surfaces is not considered throughout this manuscript because it exceeds the scope of this work and in principle would not change the general findings as believed by the authors.

The crude oils were sonicated with the montmorillonite clay over 3 days. Only then a viscosity decrease was obtained for the presented samples. By combusting the liquid phase, a MMT500 solubility of 1.1 to 1.2% and 0.6 to 0.7%wt was determined for the Pennsylvania and Colorado crude oils, respectively (see also [Supplementary Material](#)). The exact time of sonication might influence the obtained experimental results. However, the given protocol is as good as it can be, and delivers reliable results even for these industrial samples.

**Experimental methods** Rheology experiments were conducted on a MCR302 and MCR501 from Anton Paar [25], <http://www>.

**Table 1** Clay particles from Südchemie/Rockwood

Name	Abbreviation	Diameter [nm]	Thickness [nm]
Laponite RD	LRD30	30	1
Laponite OG	LOG80	80	1
Laponite WXFN	WXFN140	140	1
Montmorillonite EXM 757	MMT500	500	1

[anton-paar.com/us-en/products/group/rheometer/](http://anton-paar.com/us-en/products/group/rheometer/). The MCR302 could theoretically detect ten times lower viscosities than the MCR501. The storage and loss moduli  $G'$  and  $G''$  were measured using a Couette cell that could also be mounted on a SANS instrument with an outer diameter of 50 mm and an inner diameter of 49 mm and a height of 60 mm. The large volume and surface supported much more sensitive measurements that were needed in the case of the very fluid samples. All measurements took place in the linear regime with a strain of  $\gamma = 1\%$  (strain controlled); they were conducted in a frequency sweep from higher to lower frequencies (630 to  $10^{-3}$  rad/s) without further pretreatment. The complex viscosity was calculated on the basis of  $\eta^* = (G' + iG'')/(i\omega)$ . Due to the high viscosities of the crude oils at low temperatures, they were characterized in a cone-plate geometry with 5 cm diameter and  $1^\circ$  inclination angle. The strain amplitude was  $\gamma = 1\%$ . All crude oils were measured at constant shear frequency  $\omega = 10$  rad/s from higher to lower temperatures. The rheological SANS measurements were conducted under steady shear with given shear rates of 0.1, 1, 10, and  $100 \text{ s}^{-1}$ .

Small-angle neutron scattering (SANS) measurements were conducted on KWS1 [26, 27] and KWS3 [28, 29] at the FRM-II of the Heinz Maier Leibnitz Zentrum in Garching. The rheometer was installed for mainly tangential observations, where the alignment of the clay particles could be studied, but radial measurements were conducted as well. The neutron wavelength was 0.5 nm for KWS1 and 1.28 nm for KWS3. KWS1 is a classical pin-hole SANS for a dynamic  $Q$ -range from approx.  $3 \times 10^{-2}$  to  $5 \text{ nm}^{-1}$ . KWS3 uses a focusing mirror that focuses on the detector to reach lower  $Q$  from  $5 \times 10^{-4}$  to  $5 \times 10^{-2} \text{ nm}^{-1}$ . On KWS3, we went off-center with the detector in order to reduce the background of the primary beam. Furthermore, we had to apply a prism correction [30] due to the tangential geometry with the large wavelengths. All of this resulted in a  $Q$ -range of approx.  $10^{-2}$  to  $5 \times 10^{-2} \text{ nm}^{-1}$ . Absolute calibration was done as good as possible, since the sample thickness in the tangential geometry is not known to a high precision.

## Theory

**Theory of particles** The viscosity modification of simple fluids by spherical particles is well studied and well understood. While at low concentrations, the simple law of Einstein<sup>3</sup> is the essential result, i.e.,  $\eta_{\text{rel}} = 1 + 5/2 \phi$ , the focus lies on oblate particles. For platelets we would simply summarize the

viscosity modification as [6]:

$$\eta_{\text{rel}} = \frac{\eta}{\eta_0} = \left[ 1 - \frac{\phi}{1 - c\phi} \right]^{-0.68D/t} \quad (1)$$

The exponent is given by the platelet diameter  $D$  and the thickness  $t$ , i.e., the aspect ratio. The crowding factor  $c = \phi_c^{-1} - 1$ , would deviate from the maximal packing of platelets ( $c \approx 0$ ) due to percolation [7] to a still small value of  $\phi_c = 4.2(t/D)\ln(D/t)$  in the range of 0.2. The essential result of equation 1 is that (a) the viscosity always increases with increasing particle concentration, and that (b) the relative viscosity is weakly dependent at small particle concentrations. For particle concentrations of 1%, the relative viscosity could approximately double, and for sure could not explain factors of more than 10. Crossing over to the gel state, the system becomes viscoelastic with the proportionality of the complex shear modulus being:

$$G \sim (\phi - \phi_c)^\gamma \quad (2)$$

with the exponent  $\gamma$  being in the range of 0.8 to 2. Since the already defined critical concentration  $\phi_c$  depends rather weakly on the platelet diameter  $D$  and is much bigger than the actual particle concentration, equation 2 would predict a rather constant modulus. Again, the pure geometric consideration breaks down, and more advanced theories are needed.

**Theory of lamellar membranes** Another theory was developed for lamellar systems of membranes in a fluid medium [31]. We interpret the lamellar arrangement of the clay particles and/or sheets as the dominating structure and refer to it by the index 1. In microemulsions, the thermodynamics is dominated by the behavior of the surfactant membranes only, and the same concepts hold for lamellar microemulsions [31, 32] (the reference system is the microemulsion with index 2). Such lamellar microemulsions form in the vicinity of hydrophilic planar surfaces [14] and especially in the presence of clay particles [12]. The viscosity ratio between two lamellar systems results from [31]:

$$\eta_{\text{rel}} = \frac{\eta_1}{\eta_{\text{av}}} = \frac{E_2 \Lambda_2}{E_1 \Lambda_1} \quad (3)$$

with the energetic term  $E_i$  and the Oseen tensor  $\Lambda_i$ . For the microemulsion system, the classical energy relates to undulations of the membrane and the potential given by neighboring membranes and/or the hard solid particle (all energies in units of the thermal energy  $k_B T$ , with  $k_B$  being the Boltzmann constant and  $T$  the absolute temperature):

$$E_2 = \kappa_2 k^4 + \frac{1}{\kappa_2 d_{E,2}^4} \quad (4)$$

The undulations are governed by the bending rigidity  $\kappa_2$  and the curvature of the mode with the wave vector  $k$ . The confinement energy [31]  $\gamma/k_B T$  is given by the term  $(k_B T/\kappa_2) d_{E,2}^{-4}$  with the confinement space  $d_{E,2} = 2\sqrt{2} d \approx 2d_2$  given by the membrane spacing  $d_2$ . For the clay membranes, we assume the undulation modes to be non-energetic (i.e., no thermal fluctuations) because neighboring platelets could bend off at any angle. So only the spacing matters, and we arrive at:

$$E_1 = d_{E,1}^{-4} \quad (5)$$

The thermal energy  $\kappa_1$  of the spacing term we assumed to be unity. This energy factor anyhow only enters through details between an effective potential and the real maximum excitation. The Oseen tensor is given by:

$$\Lambda_i = \frac{1}{4k\eta_{i,\text{ref}}} \cdot \left( 1 - \frac{1 + 2d_i k + 2(d_i k)^2 (1 + 2L_i k)}{(1 + 4L_i k) \exp(2d_i k)} \right) \quad (6)$$

with the viscosity  $\eta_{i,\text{ref}}$  of the fluid around the membranes in system  $i$ , and the perforation dimension  $L_i$ . On tiniest length scales ( $k \rightarrow \infty$ ), the viscosity of the medium is the only contribution. The bracket describes a peaked function with the maximum around  $k_{\text{max}} = 0.9/d_i$ , which is connected to the repeat distance  $d_i$ . Introducing perforations keeps the maximum lower and moves it to larger  $k$ . However, this maximum describes a facilitated flow along the oriented lamellae, because all terms need to be considered at the wavevector  $k$  of the critical mode connected to the platelet diameter  $D$ ,  $k = 2\pi/D$ . The ratio of the Oseen tensors  $\Lambda_2/\Lambda_1$  leaves a ratio of the reference viscosities  $\eta_{1,\text{ref}}/\eta_{2,\text{ref}} = \eta_{\text{liq.}}/\eta_{\text{av.}}$ , which refers to the viscosity of the liquid given by equations 7 and/or 8 and an arithmetic average viscosity  $\eta_{\text{av.}} = \sum \phi_i \eta_i$  of all actual liquids in the sample (further down). Keep in mind that the Oseen tensor (eq. 6) is an approximation for small membrane inertia (usually correct in this overdamped system seen by monotonously decaying NSE relaxation curves [12]), for high dilutions and infinitely thin membranes. The latter two conditions are not extremely stressed for surfactant concentrations of bicontinuous microemulsions compared to lamellar bulk systems (as for instance found in Ref. 33 and neither for the diluted clay particles).

Here we point out that the scaling of the viscosity  $\eta$  and the shear modulus  $G$  are treated in this manuscript on a similar

basis because the microscopic frequencies of the motions affect both magnitudes in the same manner, and the scaling with changing platelet diameter should be the same. Generally, from the rheology of our systems, we can confirm that we reached the gel phase where the complex viscosity  $|\eta^*|$  is proportional to the reciprocal frequency  $\omega^{-1}$  over a wide range of time scales in agreement with Reference 34. However, the arguments about membrane dominated systems for the systems discussed here seem to work for the measured complex viscosity quite well.

**Theories of multicomponent mixtures** Historically, the oil industry was highly interested in resulting viscosities from multicomponent mixtures, because the number of components in a crude oil can be overwhelming. However, the different approaches base on different model assumptions that were lost when discussions moved to industrial scale, and so often unclear statements were obtained, and the impression of heuristic character was left to the theories. Two clearly different situations have to be distinguished: a perfect lamellar system of different components  $i$  would have the average viscosity [35, 36]:

$$\eta_{\text{liq.}}^{-1} = \sum_i \frac{\phi_i}{\eta_{\text{bare},i}} \quad (7)$$

The individual volume fractions and viscosities are  $\phi_i$  and  $\eta_{\text{bare},i}$  with  $\eta_{\text{liq.}}$  being the resulting viscosity of the mixture. Contrarily, a completely random system would follow the Arrhenius formula [36, 37]:

$$\eta_{\text{liq.}} = \alpha \prod_i \eta_{\text{bare},i}^{\phi_i} \quad (8)$$

where the factor  $\alpha$  lies in the range of 1 to 10 for many systems (Supplementary Material). The physical interpretation is connected to the heat of mixing  $Q_m$  [38] according to

$$\alpha = \exp\left(-\int \frac{Q_m}{k_B T^2} dT\right) \quad (9)$$

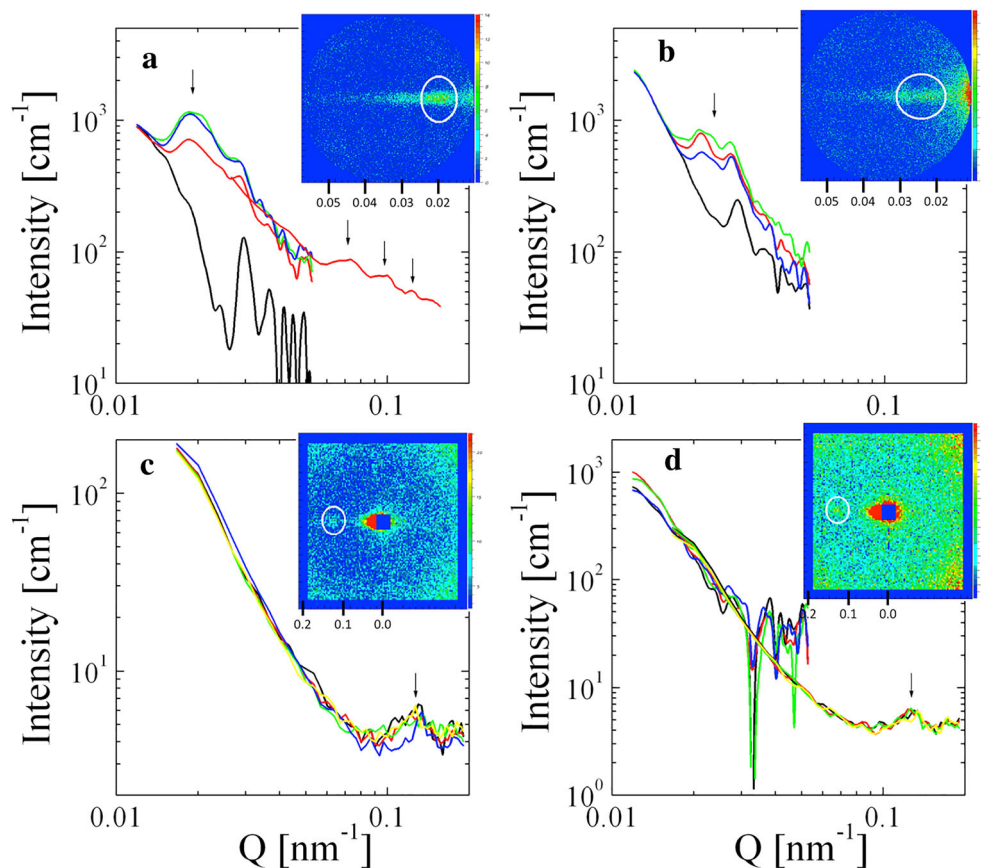
Practical ranges of  $\alpha$  are discussed in the Supplementary Material. These rules of mixing have to be considered for the membrane theories (Eqs. 3, 4, 5, and 6), if the referring system is multicomponent. Of course, the effects are essential, if rather different viscosities appear.

## Results

SANS experiments were conducted using steady shear to observe the nano-scale structure of the clay particles in simple and complex fluids (Fig. 2). The principles have already been explained elsewhere [39, 40], and the ordering of clay



**Fig. 2** SANS curves from the different clay suspensions, intensity as a function of the scattering vector  $Q$  along the velocity gradient. **a** LRD30 in  $D_2O$  for no shear (black),  $0.1\text{ s}^{-1}$  (red),  $1\text{ s}^{-1}$  (green), and  $10\text{ s}^{-1}$  (blue). **b** MMT500 in  $D_2O$  for no shear (black),  $0.1\text{ s}^{-1}$  (red),  $1\text{ s}^{-1}$  (green), and  $10\text{ s}^{-1}$  (blue). **c** LRD30 in bulk contrast microemulsion ( $D_2O$  only) for no shear (black),  $1\text{ s}^{-1}$  (red),  $10\text{ s}^{-1}$  (green),  $100\text{ s}^{-1}$  (blue), and  $0.1\text{ s}^{-1}$  (yellow). **d** MMT500 in bulk contrast microemulsion ( $D_2O$  only) for no shear (black),  $1\text{ s}^{-1}$  (red),  $10\text{ s}^{-1}$  (green),  $100\text{ s}^{-1}$  (blue), and  $0.1\text{ s}^{-1}$  (yellow). Inlays in (a, b)/(c, d) show 2d detector images from SANS at 10 m on KWS3/ at 20 m on KWS1 and indicate the Bragg peak of an oriented sample. Arrows in general indicate Bragg peaks of clay sheets with the normal direction along the velocity gradient. The vertical detector axis corresponds to the rotational axis  $\text{rot}(v)$ .



platelets can be found in the literature [41–43]. The needed length scale range is estimated through  $\ell = t/\phi = 260\text{ nm}$ , and  $Q_{\min} = 2\pi\ell^{-1}$ , which results in  $2.4 \times 10^{-2}\text{ nm}^{-1}$  (for a platelet thickness  $t = 1\text{ nm}$ , and a concentration  $\phi = 0.0038\%$  vol).

The aqueous dispersions show a clear Bragg peak at  $Q_{\text{peak}} \approx 0.02\text{ nm}^{-1}$  (Fig. 2a, b) with the sheet normal direction (and repeat unit) being oriented along the velocity gradient (scattering geometry and clay alignment depicted in the discussion section, Fig. 5). A weak second peak is distinguished at  $Q_{\text{peak}} \approx 0.03\text{ nm}^{-1}$ . The anisotropy clearly indicates a preferential lamellar order of sheets. The latter weaker peak already appears for the sample without shear. So if there is a population with a shorter repeat distance, that is already present under ambient conditions, it might form at the walls of the Couette cells. For LRD30, the clay with 30 nm diameter, we also managed to have higher order Bragg peaks of the orders 3, 4, and 5 (The second order might be missing due to the strong unwanted background that decays with increasing  $Q$ . One origin of the parasitic scattering results from the Couette cell wall roughness at grazing incidence angles.). The slight mismatch in  $Q$  might result from the incomplete prism correction of the tangential geometry that might yield a slightly lower first order Bragg  $Q_{\max}$ . Finally, the resulting repeat distance is approx.  $\ell = 300\text{ nm}$ , which seems to be right for the aqueous system.

The systems with microemulsions display only one correlation peak at  $Q = 0.13\text{ nm}^{-1}$  (Fig. 2c, d), which corresponds to repeat distances of approx.  $\ell = 50\text{ nm}$ , apart from the microemulsion correlation peak at  $Q = 0.29\text{ nm}^{-1}$ . This presumable distance of the clay platelets of approx. 50 nm underestimates the expectation for clay sheets of single platelets with nearly no holes.

Oscillatory rheological measurements were conducted to characterize the clay systems with the simple fluid water and the complex fluid of a bicontinuous microemulsion. We observed a gel-like behavior with a viscosity  $|\eta^*|$  scaling with the reciprocal frequency [34]  $\omega^{-1}$  within  $\omega = 10^{-3}$  to 50 rad/s in the linear regime ( $\gamma = 1\%$ , see Supplementary Material, also for discussion of instabilities). The measured complex viscosities at  $\omega = 1\text{ rad/s}$  are displayed in Fig. 3. For the aqueous systems, we observe an increase of the viscosity with increasing platelet diameter, while the opposite is observed in bicontinuous microemulsions. The solid lines are obtained from the discussions below and at this stage are a guide for the eye.

**Technical system** Motivated by the decreasing viscosity trend with growing platelet diameter of the microemulsion, we tried several crude oils that were available on the market as a second class of complex multicomponent fluids, and dispersed MMT500 clay in them. We present two results from crude oils

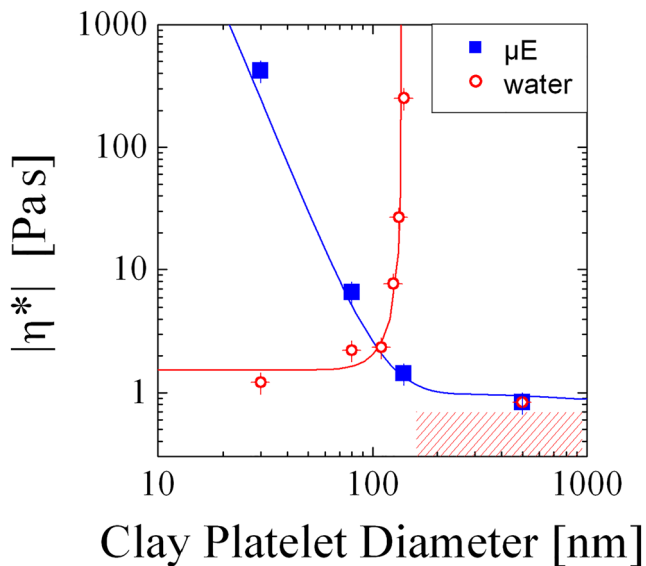
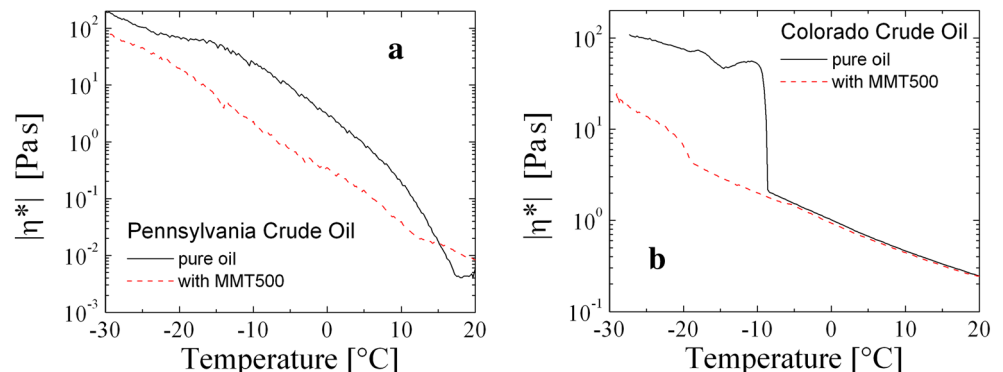


**Fig. 3** The complex viscosity of clay dispersions in water (red) and in a bicontinuous microemulsion (blue,  $\mu\text{E}$ ) as a function of the platelet diameter at 1%vol particle concentration. The solid lines result from the theory developed in Eqs. 3, 4, 5, and 6. Intermediate platelet diameters between 80 and 140 nm were obtained by particle mixing. The shaded region next to the divergence of the water systems appears due to the modified screening.

from Pennsylvania and Colorado, the cooling cycles of which we present in Fig. 4. The first oil shows a simple fluid behavior close to room temperature. At room temperature, the pure oil is more fluid than the one with clay. Below approx. 14 °C, the situation is reversed, and factors of up to 10 describe the reduction of complex viscosity when clay is dispersed. In the [Supplementary Material](#), the viscoelasticity of the two fluids can be compared on the basis of the loss tangent. Furthermore, we discuss the chemical conditions of the crude oils that display reduced viscosities. The Colorado crude oil displays a similar transition at around -8 °C, where suddenly the pure oil has a strongly increased complex viscosity. When looking in more details on the loss tangent ([Supplementary Material](#)), there seem to be more phase transitions that we cannot comment on. However, also here, the reduction of the complex viscosity can be a factor of 10.

**Fig. 4** The complex viscosity of a MMT500 suspension in **a** Pennsylvania crude oil and **b** Colorado crude oil with corresponding reference as a function of temperature.



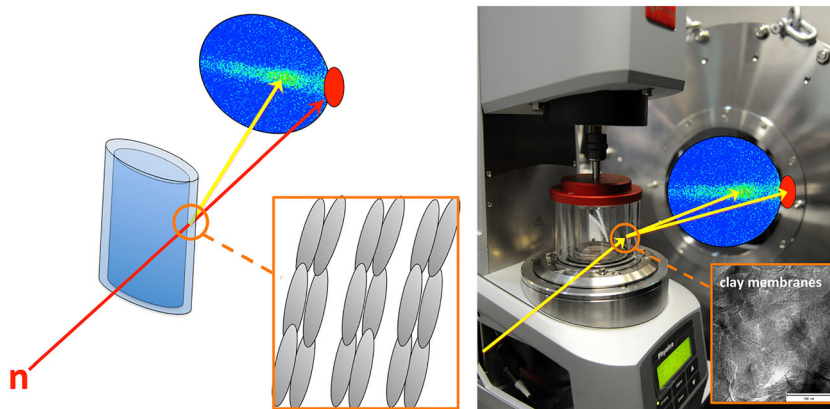
## Discussion

For the aqueous systems, we obtain from the SANS measurements a platelet spacing  $\ell$  from a Bragg peak (Fig. 5) that agrees with the simple estimation from the platelet thickness  $t$  and concentration  $\phi$  according to  $\ell = \phi/t$ . The platelet normal would be oriented along the shear gradient. Overall, this would be interpreted as regular clay sheets formed from the single platelets without large holes. The regular liquid crystalline order develops only when shear is applied [40]. This means that at rest, the alignment and spacing of the platelets is rather random, such that no coherent scattering signal is collected, while under shear. The platelets find the best arrangement by forming rather continuous clay membranes (Fig. 6, left). This is not to be confused with the formation of tactoids [39] where thicker layers of platelets form larger aggregates (laterally and in the normal direction). Face-to-face tactoid formation of montmorillonite was reported for NaCl concentrations only above approx. 1.7%wt [20, 21].

Contrarily, the platelet spacing in the microemulsion is only approx. one fifth of the arrangement in water. However, the clay arrangement displays a Bragg peak that would also only result from a regular structure. We would interpret this structure of aligned clay platelet sheets with an area coverage of only 20% that then could lead to such a spacing. A little further from facts would lead us to the interpretation that the platelet sheets have a checkerboard structure (Fig. 6, right), which might maximize the distance of the platelets due to Coulomb interactions.

The weak scattering signals of the sheets in the microemulsion systems are still visible due to fortunate side effects: In case of the aqueous systems, the scattering volume of fully covered clay sheets leads to a reasonably high scattering intensity. This is not the case for the microemulsion system, when a sheet is only covered with 20% platelets due to the surely lower degree of regular order. However, the preferential neighborhood of water ( $\text{D}_2\text{O}$ ) next to the platelets doubles the effective thickness of deuterated material. Thus, the series of layers effectively appears to be like ... HDHDCDHDH... (c for clay of 1 nm thickness, and the oil

**Fig. 5** Sketch of a rheology-SANS experiment in the tangential geometry (left). The detector for the aqueous clay dispersions has been off-center to cover a larger  $Q$ -range such that the aligned clay membranes could be observed. Rheometer installed on KWS1 (right)



(H) and water (D) domains of 10–11 nm [44]). The same configuration was not visible in film contrast where the oil and water were deuterated, because this arrangement effectively appears as ...DfDfDcDfDfD... (now c for clay, D for either oil or water, and f for surfactant film of approx. 1 nm). The local lamellar ordering of domains is still superimposed by a large fraction of bicontinuous microemulsion without preferred orientation.

From the oscillatory rheology measurements, the following observations are important: (a) At low particle concentrations of 1%wt, the aqueous samples start at viscosities of lowest values for the smaller platelet diameters of 30 and 80 nm (Fig. 3). When compared to the viscosity of water ( $10^{-3}$  Pa s), these values are already approx. 1000 times higher, which is not predicted by the classical geometrical theories (Eqs. 1 and 2). Astonishingly, the gain for the particles of 140 nm diameter lies even in the range of  $3 \times 10^5$ . The general trend of increasing viscosities agrees with Eq. 1, although the numbers do not directly lead to such high viscosity gains as experimentally found. Thus, this looks like a criticality that shall be discussed below. The montmorillonite with 500 nm diameter seems to be off this trend, and must be considered separately (also indicated by the shaded red region). (b) The systems with a bicontinuous microemulsion as a complex fluid display a steady decrease with growing platelet diameter (Fig. 3). Again, the obtained viscosities at all stages are rather high.

The most striking result from the two different fluids as medium for the clay particles is the clearly different tendency of the viscosity with growing platelet diameter.

This tendency can be seen in context with the lubrication effect [13, 31]. We have seen that the lamellae are developed better along large platelets. This would facilitate the sliding-off of the domains much more at larger platelet diameters, as observed by rheology. So the local ordering of the microemulsion as a medium serves for facilitated flow along the oriented platelets along the macroscopic flow. This leads us to a two-stage membrane interpretation with the clay platelets forming one membrane and the fluid medium having further surfactant membranes being aligned to the platelets. For both levels, we will apply the (modified) lamellar descriptions of Eqs. 3, 4, 5, and 6. The used parameters are listed in Table 2. The agreement with the measurements is quite good as seen in Fig. 3. The essential parameter is the cutoff wavelength  $k = 2\pi/D$  that is determined by the platelet diameter  $D$ .

The prefactor  $\eta_{av}$  of the aqueous system ideally takes the viscosity  $\eta_{av} = 10^{-3}$  Pa s of water while we find an approx. 10–20 times larger value. This might be due to the gel state of the system. The clay membrane distance is taken as measured from SANS, i.e.,  $d_1 = 300$  nm, while we assume the mobility of the membrane to be nearly the platelet thickness, i.e.,  $d_{E,1} = 1$  nm. That would mean that the possible overlap of the neighboring platelets confines the mobility quite strongly. Similarly,

**Fig. 6** The interpretation of the scattering experiments in terms of clay platelet structure in the two fluids: in simple fluid (left) with continuous clay membranes and in complex fluid (right) with checkerboard structure of isolated platelets (the red and blue colors indicate oil and water domains)

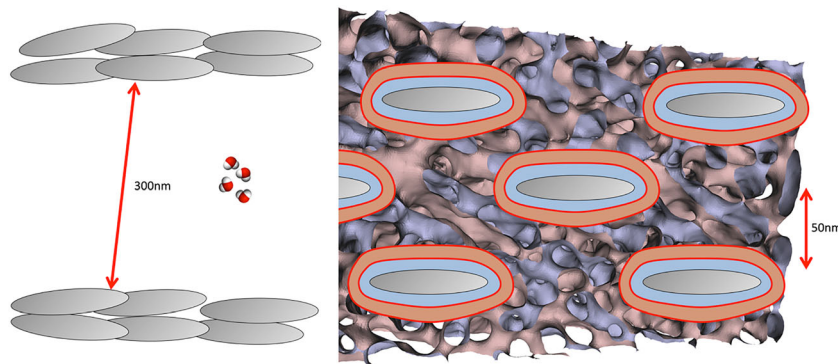




**Table 2** The parameters used to describe the rheological data.

Parameter	Aqueous system	Microemulsion system
Prefactor $\eta_{av}$	0.013 Pa s	0.022 Pa s
K	$2\pi/D$	$2\pi/D$
$d_{E,1}$	1 nm	50 nm
$d_1$	300 nm	50 nm
$L_1$	$0.1 \times D$	$1.8 \times D$
Screening $k$	$2\pi/(5 \times D)$	normal $2\pi/D$
$\kappa_2$	$1 [k_B T]$	$1 [k_B T]$
$d_{E,2}$	0.3 nm	20 nm
$d_2$	membrane modes omitted	10 nm
$L_2$		$1.8 \times D$

as above, the product  $\eta_{av}d_{E,1}^4$  determines the prefactor of the curve and leaves some room for interpretation. The residual holes in the clay membrane we assumed to be small, i.e.,  $L_1 = 0.1D$ . At this level, the exact value does not play a role. The screening  $k$  in the Oseen tensor we had to assume according to a larger stiffness within the clay patchwork, i.e.,  $k = 2\pi/(5D)$  contrarily to the unchanged model of Gov [31]. In agreement with the small freedom of normal undulations, the patchwork generates longer wavelength modes as assumed from a single platelet. This modification is responsible for the location of the divergence of the viscosity at  $D = 140$  nm, and seems to be confirmed by the detailed measurements with smaller steps in  $D$ . The experimental evidence gives us confidence for that interpretation. The secondary fluid properties we needed to treat similarly to microemulsion expressions, and found 2 simple parameters: The degree of freedom relates to water molecules with an approximate size or distance of  $d_{E,2} = 0.3$  nm [45] and the thermal energy  $\kappa_2 = 1k_B T$ . The undulation term  $\kappa_2 k^4$ , and the Oseen tensor with the other parameters  $d_2$  and  $L_2$  relate to membrane specific properties and are omitted. So the exact value  $1/(\kappa_2 d_{E,2}^4)$  also enters the prefactor of the overall curve and leaves more room for interpretations.

The prefactor  $\eta_{av}$  of the microemulsion system ideally takes the medium viscosity  $\eta_{av} = 10^{-3}$  to  $10^{-2}$  Pa s of the main fluids, while we find a clearly larger value. As we discuss on Eqs. 7 and 8, there can easily be factors of up to approx. 10 occurring due to the membrane properties, for instance an in-plane viscosity, or due to imperfections like perforations in the lamellar structure [46]. The exact value of  $\eta_{av}$  shifts the whole curve up or down in the logarithmic presentation of Fig. 3 while the following parameters mostly determine the exact shape. The spacing of the platelet membrane was measured to take the value  $d_1 = 50$  nm that we transferred to the freedom of the membrane to move in the normal direction, i.e., also  $d_{E,1} = 50$  nm. This means that the high dilution of 20% within the effective membrane possibly leaves enough freedom for that. This parameter as it is also enters the absolute prefactor of the whole curve. It is the most uncertain parameter of the

whole interpretation. The typical dimension for holes we estimate by a regular quadratic arrangement of circular disks to be  $L_1 = 1.8D$ . The exact value determines the rather low slope at the end of the curve for  $D > 200$  nm. The screening  $k$  in the Oseen tensor we leave with the original value of  $k = 2\pi/D$ , while for the aqueous system, we had to modify it. The secondary membranes are given by the microemulsion that has the structural repeat distance of  $d_2 = 10$  nm [44]. The bare bending rigidity  $\kappa_2$  takes the value of  $1k_B T$  [47]. The maximum amplitude is connected to the next neighbors, i.e.,  $d_{E,2} = 20$  nm. The only perforations of the near surface lamellar structure can only arise from the clay structure, i.e., also  $L_2 = 1.8D$ . This magnitude does not reflect in the curve shape.

The basic difference to previous publications [48] is the explicit omission of the thermal fluctuations of the clay membranes (Eq. 5) such that now only the undulation amplitude  $d_{E,1}$  enters the prefactor with some room for interpretation. The level of the contributing factors could be rationalized now. Furthermore, in the old interpretation, the clay content was taken as volume percentage. This changed the picture of single layer platelets in the aqueous medium contrarily to 3-nm thick tactoids previously assumed, and lead to a much lower density of platelets also for the microemulsion system. However, the drawn scenario did not change at large.

The main result of this modeling is the fact that the clay sheets effectively form membranes that determine the rheological response of the overall system. In the case of the simple liquid water, the clay membrane is the only important structure, while in the case of microemulsions, a secondary lamellar structure next to the platelets comes into play. This secondary structure and the difference in the clay structure (tight sheets or low density checkerboard structure) make the difference in the tendency of the viscosity with the platelet diameter. For the microemulsion system, we connect this tendency with the lubrication effect.

The observed lowest viscosities of the aqueous system are only amplified by a factor of approx. 100 at smallest platelet diameters (30 and 80 nm), while the same happens for the microemulsion system at 140 and 500 nm platelet diameter. Already, these amplifications are beyond the simple geometric particle theories for viscosities. But the highest measured viscosities exceed these findings dramatically. For the simple fluid, they are found for platelet dimensions around 140 nm due to the modified screening (divergence of  $\Lambda_1$  with the 5-fold lower cut-off  $k$  in Eq. 6). For the microemulsions, they are found for smaller platelet diameters where the lamellar structure of the complex fluid is not yet developed well enough and disturbs the facilitated flow. Also, the high viscosities are important for applications for instance in the food industry. The restructuring of the complex fluid next to the platelets is not to be confused with classical boundary layer conditions [49].

The breakdown of the sharp viscosity increase at around 140 nm towards larger platelet dimensions is observed for the



MMT500 platelets (shaded region in Fig. 3). Here, the viscosity takes the lowest values that we obtained for the other clay containing samples. The breakdown is connected to the modified screening. If the lateral correlations considerably exceed the normal repeat distance of the clay membranes, the guidance of the fluid by the membranes seems to overwhelm everything. In this sense, the system becomes similar to a complex fluid where the membranes with large correlation lengths simply guide the fluid.

The second class of complex fluids, i.e., the technical system of crude oils, needs some additional thoughts to be discussed. We know that two different effects for higher viscosities at cooler temperatures compete [50, 51] (see also [Supplementary Material](#)). The flocculation happens between approx. 100 and 0 °C and results from pi-stacking of aromatic fractions. This fraction remains at intermediate viscosities. The wax crystallization happens below approx. 0 °C and causes real solid fractions. Apart from that, there are shorter aliphatic molecules, which stay liquid in our experimental window. The crude oils do not tend to phase separate, which might result from mediating molecules with aromatic and aliphatic properties—similar to surfactants in microemulsions. In the [Supplementary Material](#), we try to argue that the higher amounts of mediating molecules support the formation of lamellar phases, which supports the observed effects. Furthermore, we assume that one component wets the clay particles.

The discussion about flocculation and crystallization causes highly different viscosities that have not been considered for the two examples of water and the microemulsion. The Equations 7 and 8 deal with multicomponent mixtures where the membrane properties are not necessarily dominant anymore [31]. One of them assumes a layered structure while the second one deals with random mixing. A simple example displays the two different ways of mixing: We have a symmetric 2-phase system ( $\phi_i = 0.5$ ) with viscosities of  $\eta_0$  and  $100\eta_0$ . The random system has a viscosity of  $10\alpha\eta_0$ , while the ordered system has a viscosity of  $1.98\eta_0$ . We believe that the domains in the crude oils can be aligned by the clay particles, which would explain the rather different viscosities at low temperatures. As for the membrane-dominated systems, a layered structure allows for layer-wise movements along the domains (and clay particles) without restructuring the domains.

## Conclusions

The development of viscosity modifications has a long history and always had an industrial background [1, 2]. Solid particles are a simple and cheap way of obtaining the desired results. Not always, a viscosity increase has been obtained with respect to another reference state [46]. But most of these studies with applications in mind were performed at rather high particle concentrations. However, we focused on particle concentrations of 1%wt and below. Starting from

the very first concepts of solid particles in a fluid, a rather low viscosity increase is predicted [3]. This goes in line even with more complicated theories, where the solid particles serve as a kind of barrier [6, 7]. When introducing complex fluids, the effect of near-surface lamellar ordering is observed [13], which seems to be stable under flow conditions [46]. This in turn, can serve for a facilitated flow called the lubrication effect [12, 31]. The idea behind is that layered structures allow for a facilitated flow contrarily to less ordered structures. Using neutron spin echo measurements, we found that clay particles with finite size can increase the mobility of the fluid when the platelet diameters are larger, while for smaller platelet sizes, the degree of ordering seems to be too low [12]. This leads us to the rheology study of clay particles in the simple fluid water and a bicontinuous microemulsion. The level of the viscosities was higher than simple theories would estimate, and trends of the viscosity with platelet diameter were different for the two fluids. The microemulsion system goes in line with the lubrication effect: Higher platelet diameters lead to smaller viscosities. This motivated us to study crude oils as a second class of complex fluids with clay particles, and a low temperatures lower viscosities were found for the clay-loaded oils. Presumably, a layering of domains was also induced by the particles as well. Apart from complex fluids, it is known that the lowest loss or highest efficiency of a flow field is achieved by the *laminar* flow [52]. This flow field describes a layer-wise sliding of the fluid without turbulences or curls. In this sense, it can be expected from complex fluids as well that if they flow layer-wise on the nano-scale, the resulting overall viscosities are low in contrast to random domains that would cause less evenly motions. Until now, the studied liquids consisted of components with very similar viscosities. Therefore, the rearrangement of domain structures left the viscosity essentially unchanged, and the highly desired case of viscosity reduction was not found. The concept of domain structure changes in the presence of clay particles was thoroughly discussed in Ref. 53. Thus, the pumping of crude oils could be facilitated by adding clay. Apart from low viscosities, we found conditions of extremely high viscosities at the low particle concentrations of 1%. This in turn could be interesting for the food industry.

**Acknowledgements** We thank Helmut Coutelle from the former Rockwood section, Moosburg, for his kind provision of clay samples. We thank Stefan Grumbein, formerly from Technical University Munich, Garching, Germany, for performing measurements on the more sensitive MCR302. We thank our chemical analysis division ZEA-3, in particular Sabine Willbold and Michael Krininger for chemical analysis support. This analysis was supervised by Jürgen Allgaier.

**Funding information** This work was supported by a State Research Grant in 2013 of LEPL Shota Rustaveli National Science Foundation Young Scholars scientific-research internship abroad.

## Compliance with ethical standards

**Conflict of interest** The authors declare that they have no conflict of interest.

**Open Access** This article is distributed under the terms of the Creative Commons Attribution 4.0 International License (<http://creativecommons.org/licenses/by/4.0/>), which permits unrestricted use, distribution, and reproduction in any medium, provided you give appropriate credit to the original author(s) and the source, provide a link to the Creative Commons license, and indicate if changes were made.

## References

- Fischer P, Windhab EJ (2011) Rheology of food materials. *Curr Op Coll Interf Sci* 16:36–40. <https://doi.org/10.1016/j.cocis.2010.07.003>
- Shah DO, Schechter RS (1977) *Improved Oil Recovery by Surfactant and Polymer Flooding*. Academic Press, New York
- Einstein A (1906) Eine neue Bestimmung der Moleküldimensionen. *AdP* 19:289–306 and A. Einstein (1911) Berichtigung zu meiner Arbeit: “Eine neue Bestimmung der Moleküldimensionen”. *AdP* 34:591–592
- Hoffmann S, Koos E, Willenbacher N (2014) Using capillary bridges to tune stability and flow behavior of food suspensions. *Food Hydrocoll* 40:44–52. <https://doi.org/10.1016/j.foodhyd.2014.01.027>
- Mourchid A, Delville A, Lambard J, LeColier E, Levitz P (1995) Phase diagram of colloidal dispersions of anisotropic charged particles: equilibrium properties, structure, and rheology of laponite suspensions. *Langmuir* 11:1942–1950. <https://doi.org/10.1021/la00006a020>
- Santamaría-Holek I, Mendoza CI (2010) The rheology of concentrated suspensions of arbitrarily-shaped particles. *J Colloid Interface Sci* 346:118–126. <https://doi.org/10.1016/j.jcis.2010.02.033>
- Bicerano J, Douglas JF, Brune DA (1999) Model for the viscosity of particle dispersions. *J Macromol Sci C* 39:561–642. <https://doi.org/10.1081/MC-100101428>
- Strey R (1994) Microemulsion microstructure and interfacial curvature. *Colloid Polym Sci* 272:1005–1019. <https://doi.org/10.1007/BF00658900>
- Leaver MS, Olsson U, Wennerström H, Strey R, Würz U (1995) Phase behaviour and structure in a non-ionic surfactant–oil–water mixture. *J Chem Soc Faraday Trans* 91:4269–4274. <https://doi.org/10.1039/FT9959104269>
- Rehage H, Hoffmann H (1991) Viscoelastic surfactant solutions: model systems for rheological research. *Mol Phys* 74:933–973. <https://doi.org/10.1080/00268979100102721>
- Chen C-M, Warr GG (1992) Rheology of ternary microemulsions. *J Phys Chem* 96:9492–9497. <https://doi.org/10.1021/j100202a077>
- Lipfert F, Holderer O, Frielinghaus H, Appavou M-S, Do C, Ohl M, Richter D (2015) Long wavelength undulations dominate dynamics in large surfactant membrane patches. *Nanoscale* 7:2578–2586. <https://doi.org/10.1039/C4NR06278G>
- Frielinghaus H, Kerscher M, Holderer O, Monkenbusch M, Richter D (2012) Acceleration of membrane dynamics adjacent to a wall. *Phys Rev E* 85:041408. <https://doi.org/10.1103/PhysRevE.85.041408>
- Kerscher M, Busch P, Mattauch S, Frielinghaus H, Richter D, Belushkin M, Gompper G (2011) Near-surface structure of a bicontinuous microemulsion with a transition region. *Phys Rev E* 83:030401. <https://doi.org/10.1103/PhysRevE.83.030401>
- Sottmann T, Strey R (1997) Ultralow interfacial tensions in water–*n*-alkane–surfactant systems. *J Chem Phys* 106:8606–8615. <https://doi.org/10.1063/1.473916>
- Xu M, Liu H, Zhao H, Li W (2013) How to decrease the viscosity of suspension with the second fluid and nanoparticles? *Sci Rep* 3: 3137. <https://doi.org/10.1038/srep03137>
- Stefanescu EA, Dundigalla A, Ferreira V, Loizou E, Porcar L, Negulescu I, Garnaio J, Schmidt G (2006) Supramolecular structures in nanocomposite multilayered films. *Phys Chem Chem Phys* 8:1739–1746. <https://doi.org/10.1039/b517880k>
- Hermes HE, Frielinghaus H, Pyckhout-Hintzen W, Richter D (2006) Quantitative analysis of small angle neutron scattering data from montmorillonite dispersions. *Polymer* 47:2147–2155. <https://doi.org/10.1016/j.polymer.2006.01.059>
- Hendricks SB (1941) Base exchange of the clay mineral montmorillonite for organic cations and its dependence upon adsorption due to van der Waals forces. *J Phys Chem* 45:65–81. <https://doi.org/10.1021/j150406a006>
- Rand B, Pekenc E, Goodwin JW, Smith RW (1980) Investigation into the existence of edge-face coagulated structures in Namontmorillonite suspensions. *J Chem Soc Faraday Trans* 76:225–235. <https://doi.org/10.1039/F19807600225>
- Heath D, Tadros TF (1983) Influence of pH, electrolyte, and poly (vinyl alcohol) addition on the rheological characteristics of aqueous dispersions of sodium montmorillonite. *J Colloid Interface Sci* 93:307–319. [https://doi.org/10.1016/0021-9797\(83\)90415-0](https://doi.org/10.1016/0021-9797(83)90415-0)
- Byelov D, Frielinghaus H, Holderer O, Allgaier J, Richter D (2004) Microemulsion efficiency boosting and the complementary effect. 1. Structural properties. *Langmuir* 20:10433–10443. <https://doi.org/10.1021/la049317t>
- Fan H, Resasco DE, Striolo A (2011) Amphiphilic silica nanoparticles at the decane–water interface: insights from atomistic simulations. *Langmuir* 27:5264–5274. <https://doi.org/10.1021/la200428r>
- Chen C, Zhang N, Li W, Song Y (2015) Water contact angle dependence with hydroxyl functional groups on silica surfaces under CO<sub>2</sub> sequestration conditions. *Environ Sci Technol* 49:14680–14687. <https://doi.org/10.1021/acs.est.5b03646>
- Rogers S, Kohlbrecher J, Lettinga MP (2012) The molecular origin of stress generation in worm-like micelles, using a rheo-SANS LAOS approach. *Soft Matter* 8:7831–7839. <https://doi.org/10.1039/C2SM25569C>
- Feoktystov AV, Frielinghaus H, Di Z, Jaksch S, Pipich V, Appavou M-S, Babcock E, Hanslik R, Engels R, Kemmerling G, Kleines H, Ioffe A, Richter D, Brückel T (2015) KWS-1 high-resolution small-angle neutron scattering instrument at JCNS: current state. *J Appl Crystallogr* 48:61–70. <https://doi.org/10.1107/S1600576714025977>
- H. Frielinghaus, A. Feoktystov, I. Berts, G. Mangiapia (2015) KWS-1: Small-angle scattering diffractometer. *J. large-scale res. facil.* <https://doi.org/10.17815/jlsrf-1-26>
- Kentzinger E, Dohmen L, Alefeld B, Rucker U, Stellbrink J, Ioffe A, Richter D, Brückel T (2004) KWS-3, the new focusing-mirror ultra small-angle neutron scattering instrument and reflectometer at Jülich. *Physica B* 350:E779–E781. <https://doi.org/10.1016/j.physb.2004.03.203>
- V. Pipich, Z. Fu (2015) *J. large-scale res. facil.* <https://doi.org/10.17815/jlsrf-1-28>
- Frielinghaus H, Holderer O, Lipfert F, Monkenbusch M, Arend N, Richter D (2012) Scattering depth correction of evanescent waves in inelastic neutron scattering using a neutron prism. *Nucl Instr Meth Phys Res A* 686:71–74. <https://doi.org/10.1016/j.nima.2012.05.064>
- Gov N, Zilman AG, Safran S (2004) Hydrodynamics of confined membranes. *Phys Rev E* 70:011104. <https://doi.org/10.1103/PhysRevE.70.011104>
- Gompper G, Schick M (1994) *Phase Transitions and Critical Phenomena* (ed. C. Domb, J. Lebowitz) Academic Press, London, 16:1–176.

33. Jaksch S, Holderer O, Gvaramia M, Ohl M, Monkenbusch M, Frielinghaus H (2017) Nanoscale rheology at solid-complex fluid interfaces. *Sci Rep* 7:4417. <https://doi.org/10.1038/s41598-017-04294-4>
34. Willenbacher N (1996) Unusual thixotropic properties of aqueous dispersions of Laponite RD. *J Colloid Interface Sci* 182:501–510. <https://doi.org/10.1006/jcis.1996.0494>
35. Awad MM, Muzychka YS (2008) Effective property models for homogeneous two-phase flows. *Exp Thermal Fluid Sci* 33:106–113. <https://doi.org/10.1016/j.expthermflusci.2008.07.006>
36. Kendall J, Monroe KP (1917) The viscosity of liquids. II. The viscosity-composition curve for ideal liquid mixtures. *J Am Chem Soc* 39:1787–1802. <https://doi.org/10.1021/ja02254a001>
37. Arrhenius S (1887) Über die innere Reibung verdünnter wässriger Lösungen. *Z Phys Chem* 1:285–298. <https://doi.org/10.1515/zpch-1887-0133>
38. Lederer EL (1931) Zur Theorie der Viskosität von Flüssigkeiten. *Kolloid Beihefte* 34:270–338. <https://doi.org/10.1007/BF02556584>
39. King HE, Milner ST, Lin MY, Singh JP, Mason TG (2007) Structure and rheology of organoclay suspensions. *Phys Rev E* 75:021403. <https://doi.org/10.1103/PhysRevE.75.021403>
40. Hanley HJM, Straty GC, Tsvetkov F (1994) A small angle neutron scattering study of a clay suspension under shear. *Langmuir* 10:3362–3364. <https://doi.org/10.1021/la00021a074>
41. Schmidt G, Nakatani AI, Butler PD, Han CC (2002) Small-angle neutron scattering from viscoelastic polymer–clay solutions. *Macromol*. 35:4725–4732. <https://doi.org/10.1021/ma0115141>
42. Schmidt G, Nakatani AI, Butler PD, Karim A, Han CC (2000) Shear orientation of viscoelastic polymer–clay solutions probed by flow birefringence and SANS. *Macromol*. 33:7219–7222. <https://doi.org/10.1021/ma9918811>
43. Ramsay JDF, Lindner P (1993) Small-angle neutron scattering investigations of the structure of thixotropic dispersions of smectite clay colloids. *J Chem Soc Faraday Trans* 89:4207–4214. <https://doi.org/10.1039/FT9938904207>
44. Endo H, Mihailescu M, Monkenbusch M, Allgaier J, Gompper G, Richter D, Jakobs B, Sottmann T, Strey R, Grillo I (2001) Effect of amphiphilic block copolymers on the structure and phase behavior of oil–water–surfactant mixtures. *J Chem Phys* 115:580–600. <https://doi.org/10.1063/1.1377881>
45. Sun CQ, Zhang X, Fu X, Zheng W, Kuo J-I, Zhou Y, Shen Z, Zhou J (2013) Density and phonon-stiffness anomalies of water and ice in the full temperature range. *J Phys Chem Lett* 4:3238–3244. <https://doi.org/10.1021/jz401380p>
46. Lipfert F, Kerscher M, Mattauch S, Frielinghaus H (2019) Stability of near-surface ordering of bicontinuous microemulsions in external shear-fields. *J Colloid Interface Sci* 534:31–36. <https://doi.org/10.1016/j.jcis.2018.09.014>
47. Holderer O, Frielinghaus H, Byelov D, Monkenbusch M, Allgaier J, Richter D (2005) Dynamic properties of microemulsions modified with homopolymers and diblock copolymers: The determination of bending moduli and renormalization effects. *J Chem Phys* 122:094908. <https://doi.org/10.1063/1.1857523>
48. Gvaramia M, Mangiapia G, Pipich V, Appavou MS, Gompper G, Jaksch S, Holderer O, Rukhadze MD, Frielinghaus H (2017/2018) Tunable viscosity modification with diluted particles: when particles decrease the viscosity of complex fluids arXiv:1709.05198, <https://arxiv.org/abs/1709.05198>
49. Berni MG, Lawrence CJ, Machin D (2002) A review of the rheology of the lamellar phase in surfactant systems. *Adv Colloid Interf Sci* 98:217–243. [https://doi.org/10.1016/S0001-8686\(01\)00094-X](https://doi.org/10.1016/S0001-8686(01)00094-X)
50. Hirschberg A, de Jong LNJ, Schipper BA, Meijer JG (1984) Influence of temperature and pressure on asphaltene flocculation. *Society Petroleum Engineers* 24:283–293. <https://doi.org/10.2118/11202-PA>
51. Misra S, Baruah S, Singh K (1995) Paraffin problems in crude oil production and transportation: a review. *SPE Production & Facilities* 10:50–54. <https://doi.org/10.2118/28181-PA>
52. Grossmann S (2000) The onset of shear flow turbulence. *Rev Mod Phys* 72:603–618. <https://doi.org/10.1103/RevModPhys.72.603>
53. Gvaramia M, Mangiapia G, Falus P, Ohl M, Holderer O, Frielinghaus H (2018) Capillary condensation and gelling of microemulsions with clay additives. *J Colloid Interface Sci* 525:161–165. <https://doi.org/10.1016/j.jcis.2018.04.032>
54. Greenwood R, Luckham PF, Gregory T (1997) The effect of diameter ratio and volume ratio on the viscosity of bimodal suspensions of polymer latices. *J Colloid Interface Sci* 191:11–21. <https://doi.org/10.1006/jcis.1997.4915>

**Publisher's note** Springer Nature remains neutral with regard to jurisdictional claims in published maps and institutional affiliations.